Helical and Dendritic Unzipping of Carbon Nanotubes: A Route to Nitrogen-Doped Graphene Nanoribbons

Alireza Zehtab Yazdi,[†] Kambiz Chizari,[†] Almaz S. Jalilov,[‡] James Tour,[*,‡,§] and Uttandaraman Sundararaj[*,†]

[†]Polymer Processing Group, Department of Chemical and Petroleum Engineering, University of Calgary, 2500 University Drive, NW, Calgary, Alberta T2N 1N4, Canada and [‡]Department of Chemistry, [§]Smalley Institute for Nanoscale Science and Technology, Department of Materials Science and NanoEngineering, Rice University, 6100 Main Street, Houston, Texas 77005, United States

ABSTRACT Bamboo structured nitrogen-doped multiwalled carbon nanotubes (CN_x-MWCNTs) have been successfully unzipped by a chemical oxidation route, resulting in nitrogen-doped graphene nanoribbons (CN_x-GNRs) with a multifaceted microstructure. The oxidation of CN_x-MWCNTs was carried out using potassium permanganate in the presence of trifluoroacetic acid or phosphoric acid. On the basis of the high resolution transmission electron microscopy studies, the bamboo compartments were unzipped *via* helical or dendritic mechanisms, which are different from the longitudinal unzipping of open channel MWCNTs. The product graphene oxide nanoribbons were simultaneously reduced and doped with nitrogen by thermal annealing in an ammonia atmosphere. The effects of the annealing temperature, time, and atmosphere on the doping level and types of the nitrogen functional groups have been investigated. X-ray photoelectron spectroscopy results indicate that a wide range of doping levels can be achieved (4−9 at %) simply by changing the annealing conditions. Pyridinic and pyrrolic nitrogen functional groups were the dominant species that were attached to the edges of the CN_x-GNRs. The GNRs, with a faceted structure and pyridinic and pyrrolic groups on their edges, have abundant nitrogen sites. These active sites could play a vital role in enhancing the electrocatalytic performance of GNRs.

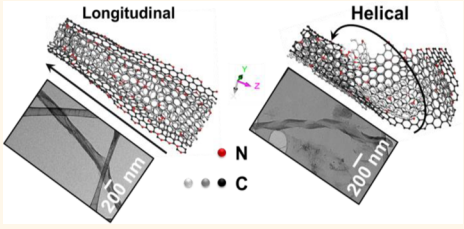

KEYWORDS: nitrogen-doped multiwalled carbon nanotubes · bamboo structures · helical/dendritic unzipping mechanisms · nitrogen-doped graphene nanoribbons

Graphene nanoribbons (GNRs), narrow elongated strips of graphene with ultrahigh aspect ratios and edge dependent properties, have recently attracted much interest as candidates to replace graphene nanosheets, particularly if synthesized by unzipping multiwalled carbon nanotubes (MWCNTs). Owing to the high available surface area, high mechanical strength, and electrical conductivity of GNRs, and the scalability of the synthesis, they have been investigated for the fabrication of composites[1,2] and for use in batteries,[3] supercapacitors[4] and fuel cells.[5]

Prior to the reports of unzipping of MWCNTs,[6−8] GNRs had been typically synthesized in minute yields and with limited width control.[9] Now, GNRs can be synthesized by unzipping of MWCNTs based on etching catalytic nanoparticles,[10] electron beam etchings,[11] potassium vapor-induced splittings,[12] and sodium/potassium intercalation.[13] The longitudinal unzipping of MWCNTs, in a mixture of potassium permanganate and sulfuric acid, was shown to produce large amounts of single graphene oxide nanoribbons (GONRs) with yields of nearly 100%.[9] Chemical oxidation in the presence of a second acid, such as phosphoric acid or trifluoroacetic (TFA) acid, was also reported to introduce lower defects into the basal plane and significantly reduces the amount of oxidants, although more oxygen functional groups will be present.[14]

Regardless of the synthesis method, the properties and performance of GNRs may dramatically change depending on the chemical and structural modifications introduced. Chemical doping, by carrier injection or extraction, is one of the most promising ways to change the electronic structure.

* Address correspondence to u.sundararaj@ucalgary.ca, tour@rice.edu.

Received for review January 19, 2015 and accepted June 1, 2015.

Published online June 01, 2015
10.1021/acsnano.5b02197

In this case, some of the carbon atoms in the sp^2 network are substituted by heteroatoms of approximately the same radius, such as nitrogen and boron, or much larger atoms, such as transition metal insertions.[15] Nitrogen and boron are often more desirable than metal doping, owing to their structural robustness. Nitrogen doping has been used in recent years to tune the properties of carbon nanotubes,[16−18] graphene nanosheets,[19−21] and nanoribbons.[22,23] For instance, the bamboo-structured CN_x-MWCNTs have been used for a wide range of applications, such as field emission devices, energy storage, gas sensors, composites, and catalysis.[17,18] One of the most outstanding potential applications found for the CN_x-MWCNTs is as electrocatalyst for oxygen reduction.[24] Owing to the active sites on their edges, CN_x-GNRs could have even more substantial performance as electrocatalysts for oxygen reduction and hydrogen evolution reactions applications.[25,26] Not all types of nitrogen species (pyridinic, pyrrolic and quaternary) would provide the doping benefits for these applications. An increase in the catalytic activity of CN_x-GNRs for oxygen reduction reaction (ORR) has been recently observed with higher concentrations of pyridinic nitrogen substituents,[27] similar to the parent CN_x-MWCNTs.[28] Further investigations are required to explore the effects of nitrogen-doped functional groups on the catalytic properties of GNRs.

Despite the exceptional properties and potential applications of CN_x-GNRs, only three methods have been published for the synthesis of CN_x-GNRs, including electrical annealing of GNRs in ammonia (NH_3),[29] chemical vapor deposition (CVD)[30] and, more extensively, longitudinal unzipping of CN_x-MWCNTs.[10,23,31,32] Similar to the synthesis of GNRs, chemical unzipping of CN_x-MWCNTs[23,31] is more preferred, due to the high yield and straightforward scalability, than using metallic nanoparticles[10] or thermal expansion techniques.[32] Silva *et al.*[23] recently studied the effect of oxidation reaction parameters, such as time, temperature and the ratio of oxidizers, on the unzipping of CN_x-MWCNTs. They found that the nitrogen atomic percent dropped from 1.56 atom % in pristine nanotubes to approximately 0.31 atom % after oxidation. Thermal annealing using decomposition of NH_3 at elevated temperatures is a promising and controllable techniques of simultaneous thermal reduction and nitrogen doping of graphene oxide (GO) nanomaterials.[19,20] This method could also be very efficient for thermal reduction and nitrogen doping of GONRs. In addition, unraveling of the bamboo compartments in CN_x-MWCNTs has been identified as a challenge in the literature with unsuccessful efforts reported to date.[23,31] Bamboo compartments, as the typical structural characteristics of CN_x-MWCNTs, can be described as many capped short carbon nanotubes that are sequentially located inside the main MWCNTs.

In the present study, CN_x-MWCNTs were synthesized through a catalytic CVD technique. They were then chemically unzipped using potassium permanganate and a second acid to obtain CN_x-GONRs. On the basis of the high resolution transmission electron microscopy (HRTEM) images, bamboo structures in the CN_x-MWCNTs were successfully unzipped through helical or dendritic unzipping mechanisms, process that are newly reported here to obtain CN_x-GONRs. To recover the properties, the CN_x-GONRs were simultaneously reduced and nitrogen-doped in NH_3 at elevated temperatures, and the products were compared to those obtained by annealing in Ar, H_2 and chemical reduction by hydrazine monohydrate. X-ray photoelectron spectroscopy (XPS) analysis also shows a 4−9 atom % nitrogen doping levels can be achieved.

RESULTS AND DISCUSSION

On the basis of prior research,[6,14] MWCNTs were unzipped using a combination of strong oxidants including sulfuric acid, potassium permanganate, and a second acid, such as phosphoric acid or TFA acid. Most recently, based on the optimized method by Higginbotham *et al.*,[14] Terrones' group studied the unzipping of CN_x-MWCNTs with slightly improvement in the reaction conditions.[23] In our previous independent study,[33] we used the original method of oxidation proposed by Kosynkin *et al.*[6] to unzip CN_x-MWCNTs with and without bamboo structures. We found that CN_x-MWCNTs with open channel structures were successfully longitudinally unzipped, while the bamboo compartments show a strong resistance to unzipping. This finding was in close agreement with the report by Silva *et al.*[23] Here, the optimized oxidation method is employed to unzip CN_x-MWCNTs that have bamboo structures. Details of the original (Method A) and optimized (Method B) oxidation methods can be found in the Materials and Methods section. In Method A, CN_x-MWCNTs were chemically oxidized/unzipped by a mixture of H_2SO_4 and $KMnO_4$. In Method B, a second acid such as H_3PO_4 or TFA was also added to the mixture for better unzipping performance.

Figure 1 shows schematics of the unzipping (Figure 1a−c) and HRTEM and scanning electron microscopy (SEM) images of the starting CN_x-MWCNTs and undoped MWCNTs (Un-MWCNTs), and GNR structures after oxidation and reduction (Figure 1d−i). CN_x-MWCNTs (Figure 1a,d) and Un-MWCNTs (Figure 1h) were synthesized using a catalytic CVD technique, where the catalyst for both was iron nitrate. The average length and diameter of Un-MWCNTs were 2.5 μm and 35 nm, respectively. CN_x-MWCNTs were of the same length, but with an average diameter of 45 nm. Averages were calculated based on the measurements of >70 nanotubes per TEM sample. As observed in many HRTEM micrographs (Figure 1d), CN_x-MWCNTs have mainly a bamboo structure,

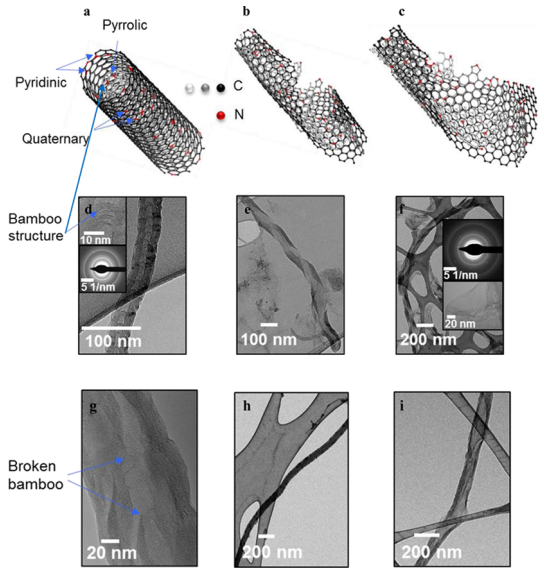

Figure 1. (a) Schematic representation of a bamboo-structured CN_x-MWCNT showing pyridinic, pyrrolic and quaternary nitrogen groups. (b and c) Helical unzipping steps to obtain a CN_x-GONR. HRTEM images of (d) a CN_x-MWCNT with bamboo compartments and selected area electron diffraction (inset), (e) a CN_x-GONR by Method B with helically unzipped structure, (f) CN_x-GNRs after nitrogen doping in NH_3 with helically unzipped structure and selected area electron diffraction (inset), (g) an oxidized CN_x-MWCNT by Method A indicating unsuccessful unzipping, but with some broken bamboo caps, (h) an Un-MWCNT with open channel structure and (i) an Un-GONR that has been longitudinally unzipped.

a characteristic that differentiates them from the usual open-channel MWCNTs (Figure 1h). The growth mechanisms of these cone-shaped cup-like structures inside CN_x-MWCNTs have been previously investigated.[17,18,34,35] There are several factors contributing to the occurrence of these structures such as catalyst, temperature and nitrogen doping. It has been found that the use of iron as the catalyst in the presence of NH_3 for the growth of CN_x-MWCNTs leads to the formation of a bamboo-like structures, whereas the use of nickel and cobalt led to the formation of open channel structures.[35] Both the base growth mechanism and the tip growth mechanism were used to explain the formation of this complex morphology.[35] It has been also reported that the CN_x-MWCNTs synthesized at lower temperatures would have mainly bamboo structures, while the synthesis temperatures above 850 °C would mostly yield amorphous carbon or random nanodomains of carbon with high nitrogen content.[17,18,35] Experimental investigations revealed that the nanotubes with a bamboo-like structure had a transition from a graphitic stacking of the outside layers to a disorganized and degraded crystallinity of graphite sheets in the core of the nanotube, where bamboo structures exist. After oxidation using Method B, both CN_x-MWCNTs and Un-MWCNTs were successfully unzipped, as shown in Figure 1, panels e and i, respectively. Figure 1f also shows a final CN_x-GNR structure obtained by nitrogen doping of CN_x-GONRs (*e.g.*, Figure 1e) in NH_3 at 500 °C for 2 h. Evidently, the CN_x-GNR after nitrogen doping (Figure 1f) is very similar to the CN_x-GONR (Figure 1e) with helical unzipping mechanism indicating the permanent formation of a GNR structure. The SAED patterns of the starting bamboo structured CN_x-MWCNTs and the final CN_x-GNRs are also added as insets to Figure 1d and 1f, respectively. A ring-like diffraction pattern with dispersed bright spots can be detected in both CN_x-MWCNTs and CN_x-GNRs indicating that the crystalline graphene structure became partially misorientated due to nitrogen doping. On the basis of several observations (*e.g.*, Figure 1f, inset), the SAED in the final CN_x-GNRs had more bright spots than the CN_x-MWCNTs indicating the formation of exfoliated GNRs after helical unzipping. In agreement with previous research,[6−8,14] the unzipping mechanism for Un-MWCNTs is longitudinal along the tube axis (Figure 1i). According to the recent theoretical calculations, the unzipping mechanism for single-walled carbon nanotubes (SWCNTs) strongly depends on the chirality of the nanotubes.[36−38] For instance, the crack propagation in armchair tubes follows the direction of the tube axis, while for the zigzag tubes, the crack propagation occurs along a tilted path. The chiral tubes present a mixed behavior.[36,37] The structural defects and the random distribution of chirality of each concentric graphitic shell, however, make it difficult to predict the unzipping method for normal MWCNTs. However, a few efforts have been made to produce MWCNTs with identical chiralities under special conditions.[39] CN_x-MWCNTs, containing nitrogen functional groups and bamboo compartments inside the nanotubes (Figure 1a,d), have made the prediction of unzipping mechanism even more complicated. The main observed mechanisms for these nanotubes are helical cleavage around the tube (Figure 1b,c,e,f, and Supporting Information Figure S1) and dendritic cuttings (Supporting Information Figure S2). The helical and dendritic unzipped structures have many more edges along the length of the nanoribbon than the longitudinally unzipped open channel MWCNTs. These extra edges provide additional surface area and active sites for applications in nanocomposites and electrocatalysts. Further experimental and theoretical studies will be conducted on the formation of these exceptional active edge sites and areas through helical and dendritic unzipping mechanisms. Here, the effect of the intrinsic nature of bamboo compartments on the formation of these active sites in the final nitrogen-doped graphene nanoribbons must be considered. The ideal condition would be to have GNRs completely and tightly helically or dendritically opened with fully exfoliated morphologies, because then all edges could contribute to the interactions. The resultant 3D GNR structures are generally a few layers of graphene

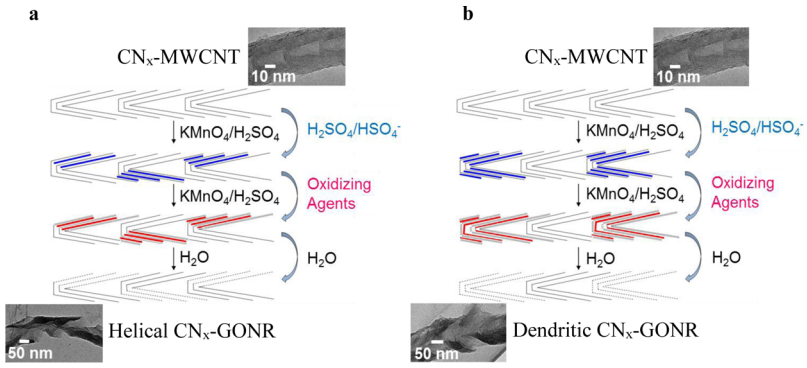

Figure 2. Proposed (a) helical and (b) dendritic unzipping mechanisms of CN_x-MWCNTs with original bamboo structures to obtain CN_x-GONRs.

(Figure 1e, and Supporting Information Figures S1 and S2, light gray), although the 2D HRTEM images look thicker in some parts of the structure (Figure 1e, Supporting Information Figures S1 and S2, dark gray). It was frequently observed *via* the HRTEM imaging process that once the entire body of the GNRs was exposed to the electron beam, beam-induced movement in the GNRs results in making some portions appear thicker (or darker) than the other portions.

The surface chemistry of CN_x-MWCNTs and the geometrical complexity of their structures play important roles in helical or dendritic unzipping. The distribution and type of the nitrogen functional groups (pyridinic, pyrrolic and quaternary) found through the nanotubes' structure will affect the reactivity of the nanotubes during oxidation, and thus, unzipping may occur. Additionally, the geometrical characteristics of bamboo structures may be responsible for these complicated mechanisms. Recent theoretical studies have shown that the oxidative reaction will be significantly increased with curvature of the carbon nanotubes.[38] One can expect, therefore, that the nanotubes with bamboo compartments will be more reactive to oxidants than the open channel tubes, particularly close to the dome part of the bamboo where the curvature of the walls and the internal strains could enhance the reactivity. HRTEM microstructural studies of oxidized CN_x-MWCNTs, using Method A, showed that bamboo compartments inside the nanotubes are initially attacked by oxidants (Figure 1g, Supporting Information Figure S3), but unzipping was unsuccessful.[33]

Although the unzipping mechanism of MWCNTs has been previously proposed based on protonation of manganate ester and ketone formation,[6,14,23] this does not explain why SWCNTs cannot be chemically unzipped. The multiwalled structure appears to play an important role in unzipping initiation and propagation. Very recently, Dimiev *et al.*[40] proposed a new approach toward formation of GO based on intercalated graphite structure. Therefore, we propose the helical and dendritic unzipping mechanisms of bamboo-structured CN_x-MWCNTs according to Figure 2, panels a and b, respectively. Similar to the mechanism of GO formation, three independent steps can be identified throughout the conversion of bamboo structured CN_x-MWCNTs to helical or dendritic CN_x-GONRs. The first step begins immediately upon exposing CN_x-MWCNTs to the acidic oxidizing medium where the graphitic walls of the nanotube are intercalated by hydrosulfate anions (Figure 2). The second step is substitution of the acid intercalated species between the walls by the oxidants which is a diffusive-controlled process and significantly slower than the first step. Intercalation by hydrosulfate anions and subsequent insertion of the oxidizing agents increase the pressure between the carbon nanotube walls. Obviously, the pressure applied on bamboo compartments at the inner nanotube layers is much higher than that at the outer layers, in particular close to the dome part where the residual stresses due to the curvature of graphitic walls might even enhance the pressure. In the third step, the intercalated oxidants between the walls of nanotubes react with water which eventually results in the unzipping and exfoliation of the nanotubes. Owing to the enhanced local pressure in bamboo structures and degraded crystallinity of their graphitic walls, likely they would be broken in the initial stages of the unzipping process earlier than the outer nanotube layers, as shown in Figure 1g, Supporting Information Figure S3. Helical or dendritic mechanism may occur depending on the location where hydrosulfate anions intercalate the bamboo caps. Upon intercalation of the bamboo caps, unzipping is speculated to occur based on the dendritic mechanism (Figure 2a). However, if intercalation only occurs in one side of the caps, helically unzipped structure may be obtained (Figure 2b).

To study the oxygen and nitrogen surface functionalities, all samples were analyzed by XPS. The high resolution C 1s spectra of the original CN_x-MWCNTs and Un-MWCNTs, and their oxidized and reduced samples are given in Figure 3. It is evident that the oxidation level of CN_x-MWCNTs, by Method A (Figure 3a, C/O = 5.99), is significantly lower than that by Method B, where 4 mL of TFA acid was used

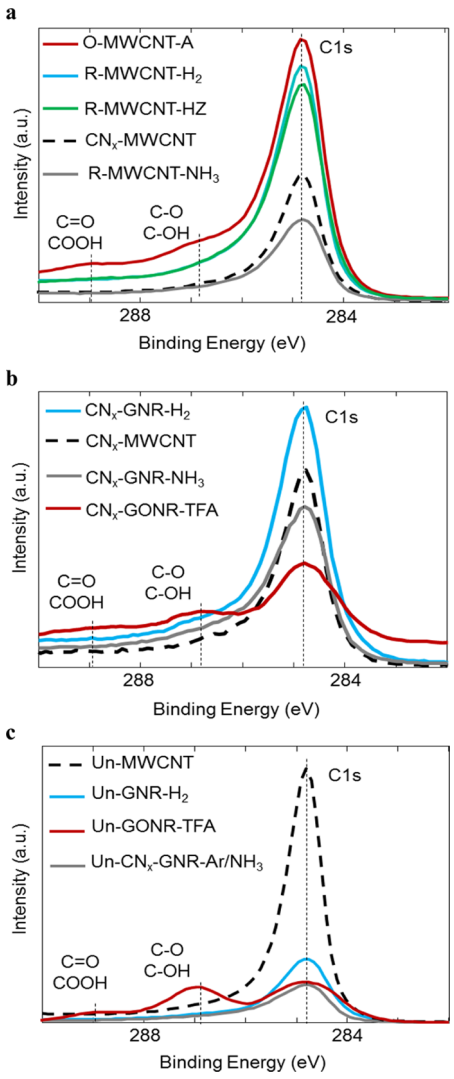

Figure 3. C 1s high resolution XPS spectra of (a) oxidized CN_x-MWCNTs by Method A (O-MWCNT-A) and reduced by hydrazine (R-MWCNT-HZ), H_2 (R-MWCNT-H_2) or NH_3 (R-MWCNT-NH_3); (b) GONRs obtained from oxidation by Method B where TFA was the second acid (CN_x-GONR-TFA) and thermally annealed in H_2 (CN_x-GNR-H_2) or NH_3 (CN_x-GNR-NH_3) and (c) undoped GONRs from oxidation of Un-MWCNTs by TFA (Un-GONR-TFA) and reduced in H_2 (Un-GNR-H_2) or Ar/NH_3 (Un-GNR-Ar/NH_3). Note: In sample CN_x-GNR-H_2 nitrogen coming from the parent CN_x-MWCNTs.

(Figure 3b, C/O = 2.29). The deconvolution of C 1s peaks, based on a Lorentz-Gauss algorithm, also indicates that the oxygen functional species in both oxidation methods exist predominantly in the form of hydroxyl (C−OH, 286.2−286.5 eV) and/or epoxy (C−O, 286.7−287.0 eV) groups and few of them are carbonyl (C═O, 287.6−287.8 eV) and carboxyl (O═C−OH, 288.8−289.1 eV) groups (Supporting Information Figure S4). Note that all spectra is calibrated with a binding energy of 284.8 eV for C═C bond. According to the generally accepted Lerf−Klinowski model for GO, hydroxyl and epoxy groups are mostly attached to the graphene basal plane, while carbonyl and carboxyl groups are presumably located at the edges.[14,23,41,42] In contrast, prior work on unzipping pristine Un-MWCNTs has shown slight changes in the C/O ratio (1.5−1.8) both with and without using a second acid, and successful unzipping has been observed.[6,14] Regarding the geometrical complexity of bamboo structures in CN_x-MWCNTs, the significant C/O ratio difference between oxidation Methods A and B can thus be attributed to the unzipping mechanisms of these nanotubes. When CN_x-MWCNTs were oxidized using only sulfuric acid and potassium permanganate *via* Method A, bamboo compartments were preserved and few internal breakages of the caps were characterized (Figure 1g, Supporting Information Figure S3). This incomplete unzipping process, also reported by Silva *et al.*,[23] could prevent further oxidization of the sp^2 carbon network, and therefore, a higher C/O ratio is obtained. Alternatively, CN_x-MWCNTs were fully unzipped by helical or dendritic mechanisms if a second acid (TFA or H_3PO_4) was added to the oxidation protocol in Method B (CN_x-GONRs-TFA). This provided the conditions for adding more oxygen species for further unzipping of the nanotubes, and thus a lower C/O ratio was achieved. Figure 3c also displays the C 1s XPS spectra of Un-MWCNTs after oxidation with added TFA (Un-GONR-TFA). This figure demonstrates the formation of larger amounts of epoxy and hydroxyl groups inside the graphene basal plane than carbonyl and carboxyl groups on the edges of Un-GONRs. According to the proposed oxidation mechanism for Un-MWCNTs, the second acid improves the chemoselectivity by minimizing the oxidation process since it prevents or retards overoxidation to the diones.[14]

To recover the conductivity properties, samples were reduced by chemical and thermal methods. The C 1s XPS spectra of the reduced samples are also shown in Figure 3. For chemical reduction, hydrazine was extensively used to reduce GO derivatives.[6,9,14,43] Thermal annealing is another promising strategy to reduce GO at elevated temperatures in inert or reducing atmospheres. Figure 3a indicates the C 1s XPS spectra of oxidized samples, by Method A, that were then reduced by hydrazine, H_2 or NH_3. Reduction by hydrazine monohydrate slightly improved the C/O ratio (from 5.99 to 7.80), whereas thermal annealing in H_2 and NH_3 at 500 °C for 2 h dramatically removed the oxygen functional groups and increased the C/O ratio to 18.22 and 29.31, respectively. Note that the shoulders attributed to the epoxy and hydroxyl groups are still detectable in the hydrazine and H_2 reduced samples, but the total oxygen content is different. The low reduction efficiency of hydrazine reagents, when compared to thermal reduction, has also been reported previously for GO and GONRs.[19,23] As indicated in the deconvoluted peaks of Supporting Information Figure S4a, the main oxygen functional groups present in product from Method A are ~11% hydroxyl

moieties, and thus, the reduction efficiency should be very low for hydrazine. On the other hand, H_2 and NH_3 are more favorable than the inert atmospheres and vacuum for thermal reduction of GO nanomaterials. H_2 and NH_3 can react and consume the residual oxygen in the reactor at high temperatures. In particular, NH_3 is proposed to be more effective than H_2 for GO since the oxygen functional groups are very reactive with NH_3 to form C−N bonds.[19] Simultaneously, the graphene structures can also be doped with nitrogen atoms, which is very useful for catalytic and electronic applications.

To further improve and optimize the reduction effect, multistep reduction may be used for some special applications.[43] The C 1s XPS spectra, for the samples that were first reduced by hydrazine and then reduced by H_2, are shown in Supporting Information Figure S5a, where a slight increase in C/O ratio (19.42) was obtained compared to reduction by H_2 only. CN_x-GONRs obtained from oxidation of CN_x-MWCNTs by Method B (TFA as the second acid) were thermally reduced with H_2 or NH_3, each at a flow rate of 100 sccm at 500 °C for 2 h (Figure 3b). Similarly, the reduction under NH_3 is more effective (C/O = 12.97) than under H_2 (C/O = 9.40), due to the high reactivity of the oxygen functional groups with NH_3. CN_x-GONRs obtained in the presence of H_3PO_4 as the second acid were also reduced in different atmospheres, including NH_3, H_2/NH_3 (20%) or Ar at 500 °C for 30 min (Supporting Figure S5b). It is obvious that NH_3 is the best reducing atmosphere for CN_x-GONRs. An increase in annealing temperature, from 500 to 700 °C, may slightly improve the reduction efficiency (C/O ratio = 9.48). Unlike the reducing atmospheres (*e.g.*, NH_3 or H_2), Ar provides an inert atmosphere and is not very effective in reduction of CN_x-GONRs, as shown in Supporting Information Figure S5b. A comparison of the C/O ratio of the reduced samples in Figures 3a,b, however, indicates that the overall reduction efficiency of the nanotubes oxidized by Method A is much higher than that of CN_x-GONRs by Method B for both NH_3 and H_2. This may be attributed to the unzipping mechanisms and distribution of the oxygen functional groups after oxidation by Methods A and B. As discussed earlier, incomplete unzipped/oxidized samples by Method A (Figure 1g, Supporting Information Figure S3) have functional groups mostly in the basal plane (hydroxyl, epoxy) and a few edge moieties, including carbonyl (3%) and carboxyl (3%) groups, were detected (Supporting Information Figure S4a). In contrast, samples oxidized by Method B showing helical (Figure 1e,f, Supporting Information Figure S1) or dendritic (Supporting Information Figure S2) unzipped structures have much higher epoxy (37%) and carboxyl (9%) groups, but almost no hydroxyl groups (Supporting Information Figure S4b). On the basis of the calculations by Gao *et al.*,[44] hydroxyl and carboxyl groups can be dissociated at lower temperatures (200−650 °C), while epoxy and carbonyl groups are much more stable and can only be removed above 1200 °C. Therefore, the higher amount of epoxy groups in the samples oxidized by Method B could be responsible for the lower reduction efficiency. Additional experiments are necessary to study the effect of increasing the reduction temperature to more than 1200 °C on the removal of epoxy and carbonyl groups. Un-MWCNTs were comparatively oxidized *via* Method B and reduced under the similar conditions, as shown in Figure 3c. Although the oxygen functional groups in undoped samples are almost the same as CN_x-GONRs (compare Supporting Information Figure S4b,c), the reduction efficiency is not very high and does not follow the same trend for H_2 and NH_3. Dilution of NH_3 with Ar may be responsible for this opposite trend.

The nitrogen content of CN_x-MWCNTs after oxidation/unzipping and reduction/postdoping in NH_3 was measured from the N 1s XPS spectra as shown in Figure 4. On the basis of the deconvoluted peaks of CN_x-MWCNTs (Figure 4a), nitrogen may incorporate into the hexagonal carbon structure in four main configurations: pyridinic (398.3−399.8 eV), pyrrolic (400.1−400.5 eV), quaternary (401.0−401.4 eV) and intercalated nitrogen molecules (404.0−405.6 eV).[17,23] The removal of nitrogen trapped inside the nanotube structure after oxidation could be an indication of successful unzipping, thus creating more edges in the structure. In agreement with the microstructural observations in Figure 1, bamboo compartments are partially affected by Method A oxidation as they have high amounts of trapped intercalated nitrogen (Figure 4b). On the other hand, oxidation by Method B appeared to remove almost all of the trapped nitrogen and no characteristic peak was observed (Figure 4c,d). The XPS peaks of nitrogen were also recently reported to have disappeared after successful unzipping of CN_x-MWCNTs without bamboo structures.[23] Comparing the nitrogen content before (2.31 atom %) and after oxidation, however, shows that the total nitrogen that remained in the structure after oxidation by Method A (1.28 atom %) was significantly lower than oxidation/unzipping by Method B (1.75−1.89 atom %). This might be due to the excessive removal of pyridinic functional groups as nitrogen rich regions by Method A (compare Figure 4b with 4c,d). The nitrogen contents of the reduced CN_x-GONRs are also shown in Figure 4e−h. Reduction by hydrazine could slightly improve the overall nitrogen content of the oxidized nanotubes, mostly in the form of quaternary and pyrrolic structures, and very little pyridinic functional groups were detected (Figure 4e). Reduction of the same sample (oxidized by Method A) in NH_3 not only removed most of the oxygen functional groups, but simultaneously, nitrogen doped the sp^2 carbon structure (Figure 4f). In this case, most of the nitrogen was

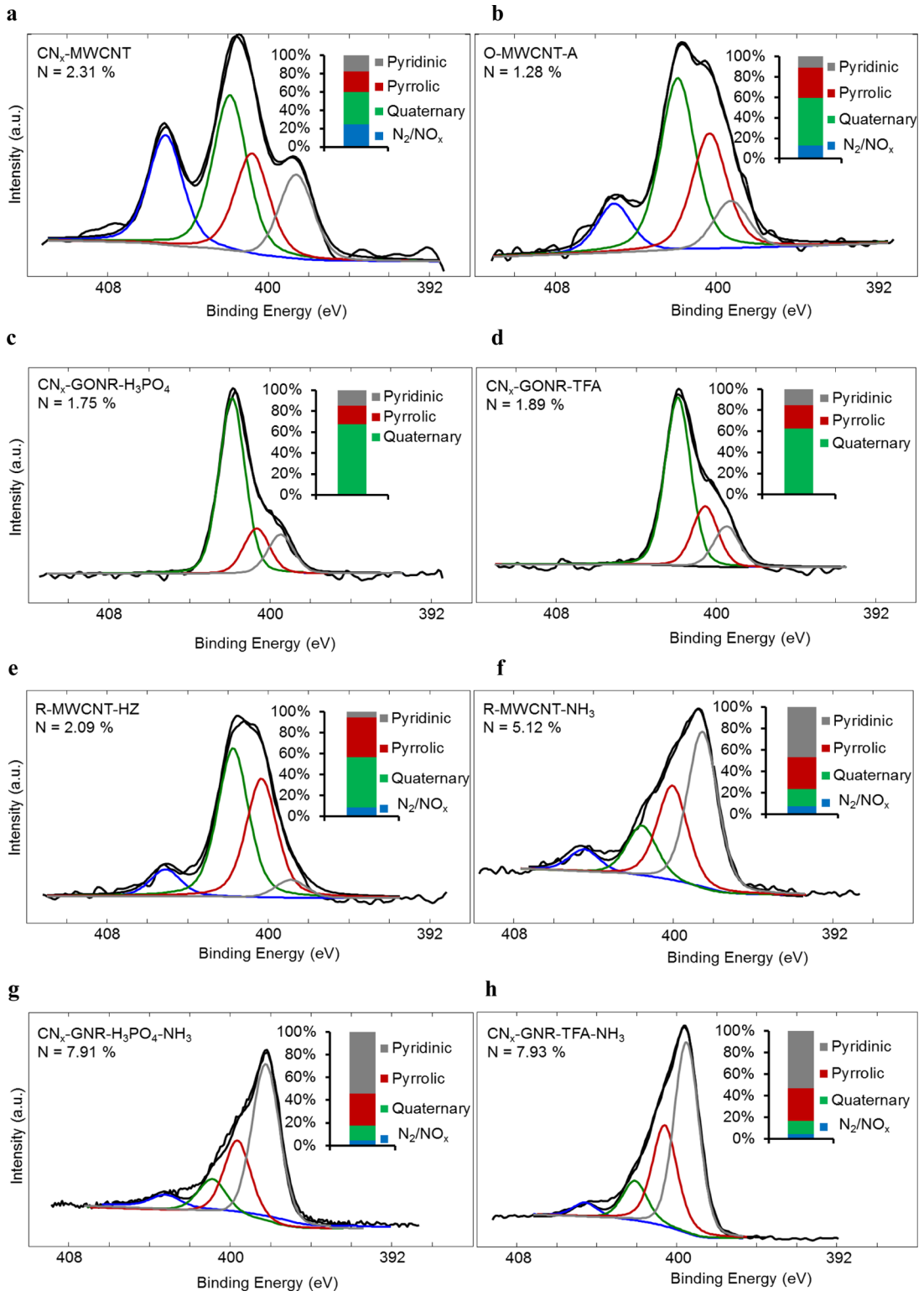

Figure 4. N 1s high resolution XPS spectra of (a) CN_x-MWCNT, (b) oxidized CN_x-MWCNTs by Method A (O-MWCNT-A), (c and d) GONRs obtained from oxidation of CN_x-MWCNTs by Method B where H_3PO_4 and TFA are the second acids, respectively. (e and f) Reduced MWCNTs by hydrazine (R-MWCNT-HZ) or NH_3 (R-MWCNT-NH_3), respectively; (g and h) CN_x-GNRs obtained by reduction of GONR-H_3PO_4 and GONR-TFA in NH_3.

pyridinic in nature. The presence of more edges in the faceted structure of unzipped samples by Method B (Figure 1e,f) increases the overall nitrogen content, peak intensity, and thus the amount of pyridinic groups (Figure 4g,h). In other words, when there is higher amount of oxygen in the CN_x-GONRs (Method B), the reactivity with nitrogen source during the doping process increases; thus, higher nitrogen

doping levels can be obtained, mainly in the form of pyridinic. This is in close agreement with the findings previously reported by Li *et al.*[19] and Long *et al.*[20] for simultaneous thermal reduction and nitrogen doping of GO. It has been found that removing the reactive oxygen groups through a prereduction of GO in H_2 at temperatures above 500 °C led to a much lower reactivity during the subsequent nitrogen doping process, and therefore, lower nitrogen content was obtained.[19] It should be noted that the nitrogen doping level and functional groups in the samples oxidized in the presence of TFA and H_3PO_4 are almost the same. Pyridinic nitrogen functional groups can be the main active sites for ORR applications.[28]

The effects of doping temperature and time on nitrogen concentration and functional groups of CN_x-GNRs were studied and the results are shown in Figure 5. All samples were annealed in Ar/NH_3 (20%) using a total gas flow rate of 100 sccm. Figure 5a indicates the effect of the doping temperature on the nitrogen doping level and the C/O ratio of oxidized/unzipped bamboo structures by Method B. It is seen that an increase in the reduction temperature, from 300 to 500 °C, results in a slight increase in the nitrogen doping level, but a significant decrease is observed from 500 to 700 °C. Here, the exposure time is 30 min. In contrast, the C/O ratio increases continuously as more oxygen functional groups are removed at higher temperatures. It can be concluded that the optimum annealing temperature for simultaneous doping and reduction of CN_x-GONRs is at 500 °C, very similar to the temperature needed for GO.[19] At higher temperatures (>500 °C), the formation of N_2 is more favorable than nitrogen atoms, thus leaving the reaction zone without participating N atoms for doping and reduction of CN_x-GONRs.[17,18] In addition, C−C bonding is reported to be more stable at higher temperatures than C−N bonding.[45] These could be the two reasons for the lower level of nitrogen doping at $T > 500$ °C.

In summary, a wide range of nitrogen doping level can be obtained for CN_x-GONRs (4−9 atom %) depending on the annealing conditions, while a limited amount of nitrogen species can be incorporated into CN_x-MWCNTs structure (~2 atom %) during the growth period. A similar trend for N atomic % and C/O ratio *vs* temperature has been observed if samples are reduced in a H_2/NH_3 (20%) atmosphere (Supporting Information, Figure S6). In addition to temperature, the effect of the reaction time on the doping level of CN_x-GONRs with unzipped bamboo structures is studied and shown in Figure 5b. The reduction temperature is 500 °C. The use of NH_3 as the nitrogen source, for 30 min, slightly increased the doping level (~9 atom %), although the nitrogen concentration slightly dropped after 1 or 2 h exposure (~8 atom %). This can also be attributed to the formation of N_2 and C−C bonding over longer time at high temperature. Unzipped

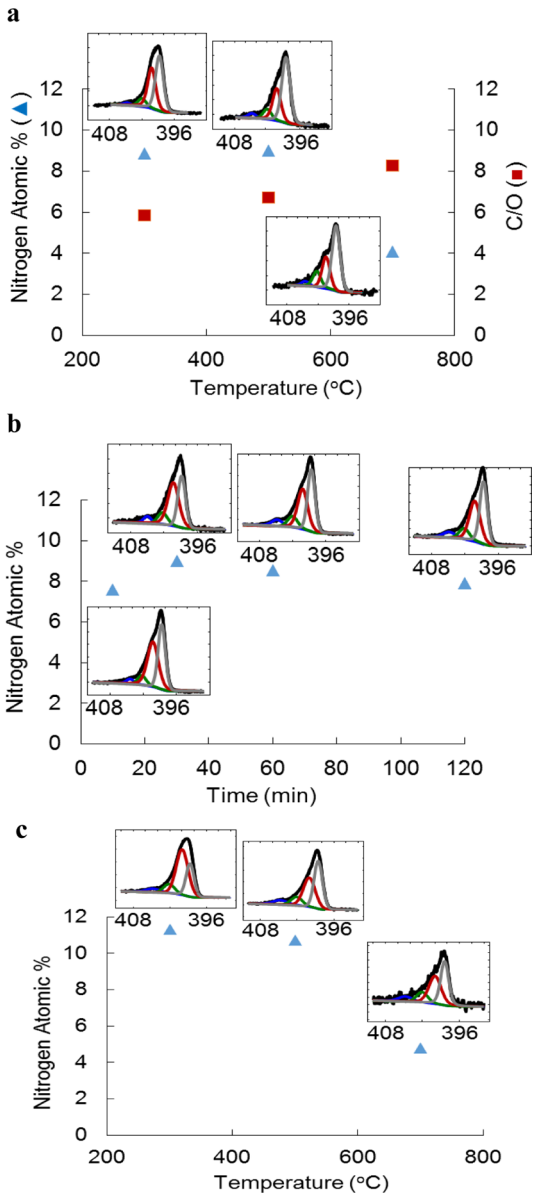

Figure 5. (a and b) Effect of doping temperature and time, respectively, on nitrogen atomic % and C/O ratio of CN_x-GNRs obtained by annealing of CN_x-GONRs. (c) Effect of doping temperature on nitrogen atomic % of Un-CN_x-GNRs obtained by annealing of Un-GONRs. All samples were annealed in Ar/NH_3 (20%).

Un-MWCNTs were also annealed in the same media of Ar/NH_3 (20%) at different temperatures (Figure 5c). Similar to CN_x-GONRs, significant changes in nitrogen atomic % are also observed in Un-GONRs after annealing at elevated temperatures (5−11 atom % in Un-CN_x-GNRs).

Structural defects of the samples, due to oxidation/unzipping and nitrogen doping, were studied by Raman spectroscopy. Raman spectra of graphitic carbon materials have three main characteristic bands, denoted as the D, G and 2D bands. The D-band, also called the "disorder-band," is representative of disorders in the sp^2 carbon network and only becomes

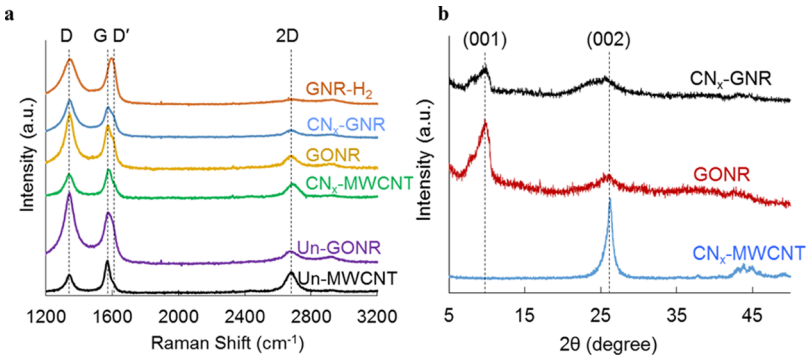

Figure 6. (a) Raman and (b) XRD spectra of MWCNTs, GONRs and GNRs samples. GNR-H_2 and CN_x-GNRs were obtained by thermal treatment of CN_x-GONRs in H_2 and NH_3, respectively, at 500 °C for 2 h.

Raman active upon loss of symmetry in the network. The G-band, which is representative of C−C bonding, is found in all Raman spectra as the signature of the graphitic network. The 2D-band is an overtone of the D-band and is sensitive to changes in the electronic structure, such as incorporation of dopants. This band is also an indication of excitation laser frequency changes in the carbon framework.[46] The Raman spectra of original MWCNTs, GONRs and CN_x-GNRs are shown in Figure 6a. An increase in the I_D/I_G ratio (0.6 to 0.96) is observed for CN_x-MWCNTs as compared to Un-MWCNTs; this is evidence of more defects in the nitrogen-doped nanotube structure. The G-band has slightly blue-shifted (1571 to 1576 cm^{-1}) and a shoulder appears on the right side of the peak, called the D′-band. This could be attributed to the substitution of some carbon atoms with nitrogen atoms, which diminishes the ordering of the graphitic network.[17] The 2D-band also becomes broader and lower in intensity in CN_x-MWCNTs, leading to the lower I_{2D}/I_G ratio. After oxidation/unzipping by Method B, both CN_x-GONRs and Un-GONRs showed a dramatic increase in their D-bands (I_D/I_G ratio) due to the oxygen groups and structural defects on the basal plane. A more significant increase in I_D/I_G ratio of the samples oxidized by Method B was observed than the samples oxidized by Method A. The D′-band peak is enhanced after oxidation, and is representative of the combined effects of nitrogen doping and the oxidation induced defects in the GNR structure. Samples reduced by H_2 and NH_3 at 500 °C for 2 h still show large I_D/I_G ratios (strong D-bands) which is in agreement with previous reports for chemically reduced GNRs[6,14] and thermally reduced and nitrogen-doped GO samples.[19] It is proposed that reduction can only increase the number of domains responsible for the D-band, but not necessarily their overall size, which is responsible for the G-band.[14] Note that due to the high level of nitrogen doping in the sample reduced by NH_3 (~9.5 atom %), the D′-band is obvious, while in the sample reduced by H_2, the D′-band almost disappears (*i.e.*, no D′ shoulder is visible). In addition, the 2D-band is very weak after reduction, particularly by H_2, as compared with the oxidized samples and the parent CN_x-MWCNTs. In the literature, the effect of nitrogen doping on the intensity of the 2D-bands (I_{2D}/I_G ratio) is still under experimental investigations. Although it has been observed that I_{2D}/I_G ratio can initially increase by decreasing the nitrogen content up to a turning point and then decrease,[17,47] there is another report that showed an opposite trend as the nitrogen content was raised to 1 atom %.[48]

To further investigate helically or dendritically unzipped structures, X-ray diffraction (XRD) patterns of the original CN_x-MWCNTs, GONRs and CN_x-GNRs were analyzed, as shown in Figure 6b. There is a very sharp graphitic (002) peak in CN_x-MWCNTs sample at 26.24° corresponding to a *d*-spacing of 3.4 Å. After oxidative intercalation of the bamboo structures and successful unzipping *via* Method B, a strong and slightly broader (001) peak in the CN_x-GONRs sample appeared at 9.78° which corresponds to a *d*-spacing of 9.1 Å. This peak is an indication of the successful unzipping and exfoliation of the graphitic layers. However, the intensity of this peak decreases after thermal treatment in the CN_x-GNRs due to reduction and probably restacking of the exfoliated layers. Note that the graphitic (002) peak in CN_x-GONR and CN_x-GNRs remains very weak and broad, indicating the permanent formation of CN_x-GNRs.

The thermal stability of the CN_x-MWCNTs and the Un-MWCNTs after oxidation and reduction was studied using thermogravimetric analysis (TGA), as shown in Figure 7 and Supporting Information Figure S8. Three different regions can be identified in the TGA results. In the first region, weight loss below 150 °C is mainly due to the evaporation of water residue which is an endothermic reaction.[23,30] The oxygen functional groups in the CN_x-GONRs and Un-GONRs were then removed in the second region between 150 and 400 °C (Figure 7a). The exothermic reaction for the CN_x-GONRs is stronger and occurred at lower temperatures (Figure 7b) than the Un-GONRs, most likely due to more structural defects from helical/dendritic unzipping and also

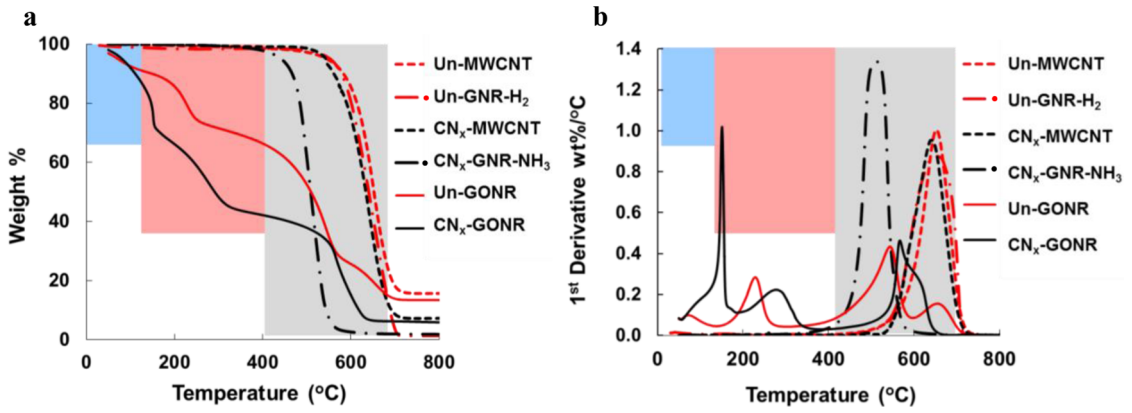

Figure 7. Comparative thermal analysis of CN_x-MWCNT and Un-MWCNT after oxidation *via* Method B and reduction using NH_3 and H_2, respectively: (a) TGA and (b) first derivative of weight % *vs* temperature.

lower crystallinity of the graphitic layers in the starting bamboo structures of the CN_x-MWCNTs. In the third region, burning of carbon materials was started from 400 up to 700 °C. The presence of nitrogen functional groups and bamboo compartments in the CN_x-MWCNTs resulted in a slightly lower degradation temperature than the Un-MWCNTs (20−30 °C). After reduction of the CN_x-GONRs in NH_3 (CN_x-GNR-NH_3), most of the oxygen functional groups were removed, although the structure is less stable at higher temperatures than the longitudinally unzipped and reduced GNR (Un-GNR-H_2). These structural defects, however, provide exceptional surface area and more active edge sites for the electrocatalytic applications. Very recently, we have shown that nitrogen/boron codoped GNRs with helically unzipped structures can compete with the current state-of-the-art Pt based electrocatalysts in all key ORR properties.[49] The ORR performance of the CN_x-MWCNTs, CN_x-GONRs, the CN_x-GNRs with helically/dendritically unzipped structure and also the Un-GNRs with longitudinally unzipped structure was also measured in an alkaline electrolyte and shown in Supporting Information, Figure S9. A clear increase in the catalytic properties of the CN_x-GNRs can be attributed to the helical and dendritic unzipping of the bamboo structures after nitrogen doping.

CONCLUSIONS

CN_x-MWCNTs with bamboo structures were successfully unzipped by a chemical oxidation method using potassium permanganate and a second acid, H_3PO_4 or TFA. HRTEM studies showed that bamboo compartments were mainly cut helically or dendritically around the nanotube axis. It was found that oxidation without using the second acid only distorted the bamboo caps and in these cases; no unzipping occurred, even though these are the preferred points of attack for oxidants, due to the internal strains. XPS results showed that nitrogen peaks, associated with the NO_x species or nitrogen intercalated molecules trapped inside the nanotube structure, almost disappeared after oxidation, indicating additional evidence of successful unzipping. GONRs were then thermally reduced using different annealing atmospheres, times and temperatures. GONRs reduction in NH_3-based atmospheres was not only more efficient than that under H_2, Ar and hydrazine, but the NH_3 further dopes the unzipped structures with nitrogen from 4 up to 9 atom %, depending on the annealing conditions. It was shown that annealing in Ar/NH_3 (20%) at 500 °C for 30 min provides the optimum balance between reduction efficiency, sufficiently high C/O ratio and a high nitrogen doping level (as high as ∼9 atom %). Doping at higher temperatures (≥700 °C) and/or for longer periods (≥1 h) significantly decreases the nitrogen concentration, as the formation of N_2 and C−C bonding are more favorable than nitrogen atoms and N−C bonding, respectively. The deconvolution of N 1s peaks from XPS spectra indicated that pyridinic and pyrrolic species are the dominant nitrogen functional groups attached to the unzipped bamboo with faceted structure. These would be the main active sites for the future electrocatalysts in oxygen reduction and hydrogen evolution reactions applications.

MATERIALS AND METHODS

Chemicals. Sulfuric acid (H_2SO_4, 95%), potassium permanganate ($KMnO_4$, 99%), trifluoroacetic acid (TFA, 99%), hydrazine monohydrate ($N_2H_4.H_2O$, 98%), diethyl ether (99%), hydrogen peroxide (H_2O_2, 30 wt % in H_2O), ammonium hydroxide (NH_4OH, 30% NH_3 basis) and ethanol (denatured, reagent) were all purchased from Sigma-Aldrich, Canada. Phosphoric acid (H_3PO_4, 85%) and hydrochloric acid (HCl, 38%) were purchased from VWR, Canada, and sodium dodecyl sulfate (100%) from J.T. Baker.

Catalytic CVD Synthesis of N-MWCNTs. *Catalyst Preparation.* Alumina-supported iron catalyst (Fe/Al_2O_3) was prepared by incipient wetness impregnation of iron nitrate (iron(III) nitrate nonahydrate, Baker Analyzed ACS grade) on an aluminum oxide support (Sasol Catalox SBa-200), followed by drying, calcination

and reduction.[17,18] The iron loading was set at 20 wt %. The catalyst was dried at room temperature for 24 h and at 100 °C for 2 h. The calcination was done at 350 °C under air flow, with a flow rate of 100 sccm for 4 h, to transform the iron nitrate precursor into its corresponding oxide. It was then ground and sieved with a small sieve to obtain a fine powder. The catalyst was further reduced in hydrogen (Praxair HY 5.0UH-T) flow, with a flow rate of 100 sccm at 400 °C for 1 h, to obtain metallic iron supported on alumina.

CN_x-MWCNTs Synthesis. CN_x-MWCNTs were synthesized *via* a CVD method using a mixture of ethane, ammonia and argon, according to the protocol of Chizari *et al.*[17,18] Ethane (Praxair ET 2.0-K) was used as a source of carbon and ammonia (Praxair AM 4.5-K) as a source of nitrogen. The alumina-supported iron catalyst was placed inside a quartz boat located inside a quartz tubular reactor, with an inner diameter of 4.5 cm, then placed inside a tube furnace (Thermo Scientific, Lindberg Blue M). The flow rates of the gases were controlled by gas flowmeters (Cole Parmer 150 mm 316 SS). The synthesis temperature, time, catalyst mass, and gas total flow rate were kept constant at 750 °C, 2 h, 0.6 g, and 150 sccm, respectively. For the purpose of comparison, undoped MWCNTs were synthesized by replacing the ammonia gas (source of nitrogen) with hydrogen; the other synthesis parameters were similar to the CN_x-MWCNTs' synthesis.

Oxidation and Unzipping of MWCNTs. *Method A.* This method is based on the original published protocol.[6] Typically, 150 mg of MWCNTs was bath sonicated for 30 min in 150 mL of concentrated H_2SO_4, followed by stirring for 2 h. Then, 750 mg of $KMnO_4$ was slowly added to the mixture. Once oily Mn (VII) oxide was seen, with a strong green metallic sheen, the addition of $KMnO_4$ was stopped until it completely dissolved. Stirring continued at room temperature for 1 h and then at 65 °C for 30 min. To stop the oxidation, the mixture was added to 120 mL of cold distilled water, containing 5 mL of H_2O_2 (30%), followed by filtration through a 5 μm PTFE membrane. At the end of the process, the black mud was washed once with HCl 20%, three times with diethyl ether, then vacuum filtered to obtain ~150 mg of flakes of GONRs.

Method B. This method is based on a published protocol.[14] In this method, 150 mg of MWCNTs was stirred in 36 mL of concentrated H_2SO_4 for 1 h. Then, 4 mL of H_3PO_4 or TFA was added and the mixture was stirred for 15 min. Note that the amount of acids required for the unzipping process in this method has been significantly reduced. Similar to Method A, 750 mg of $KMnO_4$ was slowly added and the mixture was stirred for 1 h at room temperature, followed by 2 h at 65 °C. The procedure to collect the flakes of GONRs (~150 mg) is exactly the same as in Method A.

Chemical Reduction by Hydrazine. Chemical reduction by hydrazine monohydrate was performed, as originally reported by Stankovich *et al.*,[40] for GO and was also used for GONRs.[6] A mixture of GONR powder (1 mg) and 1% aqueous SDS solution (5 mL) was homogenized with a IKA T-25 disperser at 7000 rpm for 1 h. The suspension was probe sonicated for 10 min at 75% power, followed by the addition of concentrated ammonium hydroxide (NH_4OH) and hydrazine monohydrate ($N_2H_4.H_2O$) (each agent 1 μL per 1 mL solution). The mixture was heated to 95 °C for 1 h without stirring. To remove the excess hydrazine, a tubular dialysis membrane was used for 24 h in 1% NH_4OH. Finally, reduced graphene nanoribbons were collected by vacuum filtration through a 5 μm PTFE membrane.

Simultaneous Thermal Annealing and Nitrogen Doping. GONRs powders were thermally annealed similar to the procedure proposed by Dai's group for reduction and doping of GO.[19] Samples were reduced in different media and at various temperatures and times using the same equipment for the synthesis of MWCNTs. The reducing media include argon, hydrogen, ammonia, and a combination of Ar/NH_3 (20%) and H_2/NH_3 (20%). All gases were purchased from Praxair Canada, Inc., with the same purity as used for MWCNTs synthesis. The temperatures were 300, 500, and 700 °C. The samples were also kept heated at each of these temperatures for about 10 min, 30 min, 1 h or 2 h. At the start of each reduction procedure, GONRs were put in a quartz boat inside the furnace, followed by purging with Ar at room temperature, with a flow rate of 100 sccm for about 30 min, to ensure no oxygen species were in the sealed furnace chamber. *(Caution: The presence of oxygen at an elevated temperature, particularly if H_2 is among the reducing media, may result in explosion)*. After purging Ar at room temperature, the Ar may remain closed or open, depending on the procedure. If Ar or Ar/NH_3 (20%) was the reducing agent, Ar was kept open; if H_2, NH_3 or H_2/NH_3 (20%) was the chosen medium, Ar was closed. Note that for the mixed media, including Ar/NH_3 (20%) and H_2/NH_3 (20%), the flow rate of the base medium (Ar or H_2) and NH_3 were 100 and 20 sccm (20% of the flow rate of the base gas), respectively. Once the desired medium was set up at room temperature, the furnace was heated up directly to the reaction temperature in 30 min and then kept constant at the temperature for the desired amount of time. After heating, the furnace was cooled to room temperature, in the same reduction medium. For safety purposes, Ar was purged at room temperature for 30 min with a flow rate of 100 sccm and all other gases were closed. At the end, the samples were taken out of the tube reactor and prepared for characterization.

Characterization. The overall microstructural features of MWCNTs and GNRs were studied by SEM and HRTEM. The SEM work was carried out in a Philips XL30 ESEM, using 20 kV acceleration voltage. The SEM samples were prepared by spreading the sample powders on a conductive tape located on a SEM metallic sample holder. The HRTEM was carried out in a Tecnai TF20 G2 FEG-TEM (FEI, Hillsboro, OR), at 200 kV acceleration voltage, with the standard single tilt holder. The images were captured by a Gatan UltraScan 4000 CCD (Gatan, Pleasanton, CA) at 2048 × 2048 pixels. Typically, less than 1 mg of the nanopowders was suspended in 10 mL of ethanol and the mixture was bath sonicated for 15 min. A drop of this suspension was placed on the carbon side of a standard TEM grid that was covered with a ~ 40 nm thin holey carbon film (EMS, Hatfield, PA) and placed on a filter paper to quickly dry.

To measure the elemental composition, a Physical Electronics PHI VersaProbe 5000-XPS was used to record XPS spectra. The spectra were taken using a monochromatic aluminum source, at 1486.6 eV and 49.3 W, with a beam diameter of 200.0 μm. The samples were pressed on a piece of indium foil and a double neutralization, a low energy electron beam and low energy Ar+ beam, was used during spectrum acquisition. The binding energies were reported relative to C 1s at 284.8 eV. The chamber analysis pressure was 2.0×10^{-7} Pa during acquisition. The takeoff angle was 45°. For each sample, a high sensitivity mode spectrum was taken with a wide binding energy range of 0−1350 eV (survey) to determine the surface elemental composition of the samples. Then, a narrower binding energy window, with a pass energy of 23.50 eV, was used to get high energy resolution spectra of the elements present in the sample to determine its chemical environment and quantification. The structural defects of the samples were investigated using Raman spectroscopy. The Raman spectra were recorded by a Thermo Nicolet Dispersive XR Raman Microscope with a laser radiation of 532 nm, integration of 50 s, × 10 objective and a laser power of 24 mW. X-ray diffraction (XRD) patterns were obtained using a Rigaku SmartLab X-ray Diffractometer with Cu X-ray Tube and a wavelength of 1.54059 Å.

Conflict of Interest: The authors declare no competing financial interest.

Acknowledgment. This research is financially supported by the Natural Sciences and Engineering Research Council of Canada (NSERC), Alberta Innovates Technology Futures (AITF) and Air Force Office of Scientific Research (AFOSR, FA9550-14-1-0111). Authors would like to also acknowledge the Microscopy and Imaging Facility (MIF) at the University of Calgary for their great help in HRTEM and SEM imaging and discussions.

Supporting Information Available: More HRTEM and SEM images of helical and dendritic mechanisms, XPS spectra of other processing conditions and deconvoluted peaks, TGA and ORR results of the CN_x-GNRs. The Supporting Information is available free of charge on the ACS Publications website at DOI: 10.1021/acsnano.5b02197.

REFERENCES AND NOTES

1. Khajepour, M.; Sadeghi, S.; Zehtab Yazdi, A.; Sundararaj, U. Tuning the Curing Behavior of Fluoroelastomer (FKM) by Incorporation of Nitrogen Doped Graphene Nanoribbons (CNx-GNRs). *Polymer* **2014**, *55*, 6293–6302.
2. Dimiev, A.; Lu, W.; Zeller, K.; Crowgey, B.; Kempel, L. C.; Tour, J. M. Low-Loss, High-Permittivity Composites Made from Graphene Nanoribbons. *ACS Appl. Mater. Interfaces* **2011**, *3*, 4657–4661.
3. Li, L.; Ruan, G.; Peng, Z.; Yang, Y.; Fei, H.; Raji, A.-R. O.; Samuel, E. L. G.; Tour, J. M. Enhanced Cycling Stability of Lithium Sulfur Batteries Using Sulfur-Polyaniline-Graphene Nanoribbon Composite Cathodes. *ACS Appl. Mater. Interfaces* **2014**, *6*, 15033–15039.
4. Li, L.; Raji, A. R.; Fei, H.; Yang, Y.; Samuel, E. L. G.; Tour, J. M. Nanocomposite of Polyaniline Nanorods Grown on Graphene Nanoribbons for Highly Capacitive Pseudocapacitors. *ACS Appl. Mater. Interfaces* **2013**, *5*, 6622–6627.
5. James, D. K.; Tour, J. M. Graphene: Powder, Flakes, Ribbons, and Sheets. *Acc. Chem. Res.* **2013**, *46*, 2307–2318.
6. Kosynkin, D. V.; Higginbotham, A. L.; Sinitskii, A.; Lomeda1, J. R.; Dimiev, A.; Price, B. K.; Tour, J. M. Longitudinal Unzipping of Carbon Nanotubes To Form Graphene Nanoribbons. *Nature* **2009**, *458*, 872–876.
7. Jiao, L.; Zhang, L.; Wang, X.; Diankov, G.; Dai, H. Narrow Graphene Nanoribbons from Carbon Nanotubes. *Nature* **2009**, *458*, 877–880.
8. Cano-Marquez, A. G.; Rodriguez-Macias, F. J.; Campos-Delgado, J.; Espinosa-Gonzalez, C. G.; Lopez, F. T.; Gonzalez, D. R.; Cullen, D. A.; Smith, D. J.; Terrones, M.; Vega-Cantu, Y. I. Ex-MWNTs: Graphene Sheets and Ribbons Produced by Lithium Intercalation and Exfoliation of Carbon Nanotubes. *Nano Lett.* **2009**, *9*, 1527–1533.
9. Ma, L.; Wang, J.; Ding, F. Recent Progress and Challenges in Graphene Nanoribbon Synthesis. *ChemPhysChem* **2013**, *14*, 47–54.
10. Elias, A. L.; Mendez, A. R. B.; Rodriguez, D. M.; Gonzalez, V. J.; Gonzalez, D. R.; Ci, L.; Sandoval, E. M.; Ajayan, P. M.; Terrones, H.; Terrones, M. Longitudinal Cutting of Pure and Doped Carbon Nanotubes to Form Graphitic Nanoribbons Using Metal Clusters as Nanoscalpels. *Nano Lett.* **2010**, *10*, 366–372.
11. Kim, K.; Sussman, A.; Zettl, A. Graphene Nanoribbons Obtained by Electrically Unwrapping Carbon Nanotubes. *ACS Nano* **2010**, *4*, 1362–1366.
12. Kosynkin, D. V.; Lu, W.; Sinitskii, A.; Pera, G.; Sun, Z.; Tour, J. M. Highly Conductive Graphene Nanoribbons by Longitudinal Splitting of Carbon Nanotubes Using Potassium Vapor. *ACS Nano* **2011**, *5*, 968–974.
13. Genorio, B.; Lu, W.; Dimiev, A. M.; Zhu, Y.; Raji, A. R.; Novosel, B.; Alemany, L. B.; Tour, J. M. *In Situ* Intercalation Replacement and Selective Functionalization of Graphene Nanoribbon Stacks. *ACS Nano* **2012**, *6*, 4231–4240.
14. Higginbotham, A. L.; Kosynkin, D. V.; Sinitskii, A.; Sun, Z.; Tour, J. M. Lower-Defect Graphene Oxide Nanoribbons from Multiwalled Carbon Nanotubes. *ACS Nano* **2010**, *4*, 2059–2069.
15. Banhart, F.; Kotakoski, J.; Krasheninnikov, A. V. Structural Defects in Graphene. *ACS Nano* **2011**, *5*, 26–41.
16. Gong, K.; Du, F.; Xia, Z.; Durstock, M.; Dai, L. Nitrogen-Doped Carbon Nanotube Arrays with High Electrocatalytic Activity for Oxygen Reduction. *Science* **2009**, *323*, 760–764.
17. Chizari, K.; Sundararaj, U. The Effects of Catalyst on the Morphology and Physicochemical Properties of Nitrogen-Doped Carbon Nanotubes. *Mater. Lett.* **2014**, *116*, 289–292.
18. Chizari, K.; Vena, A.; Laurentius, L.; Sundararaj, U. The Effect of Temperature on the Morphology and Chemical Surface Properties of Nitrogen-Doped Carbon Nanotubes. *Carbon* **2014**, *68*, 369–379.
19. Li, X.; Wang, H.; Robinson, J. T.; Sanchez, H.; Diankov, G.; Dai, H. Simultaneous Nitrogen Doping and Reduction of Graphene Oxide. *J. Am. Chem. Soc.* **2009**, *131*, 15939–15944.
20. Long, D.; Li, W.; Ling, L.; Miyawaki, J.; Mochida, I.; Yoon, S. H. Preparation of Nitrogen-Doped Graphene Sheets by a Combined Chemical and Hydrothermal Reduction of Graphene Oxide. *Langmuir* **2010**, *26*, 16096–16102.
21. Wang, H.; Xie, M.; Thia, L.; Fisher, A.; Wang, X. Strategies on the Design of Nitrogen-Doped Graphene. *J. Phys. Chem. Lett.* **2014**, *5*, 119–125.
22. Wang, X.; Li, X.; Zhang, L.; Yoon, Y.; Weber, P. K.; Wang, H.; Guo, J.; Dai, H. N-Doping of Graphene through Electrothermal Reactions with Ammonia. *Science* **2009**, *324*, 768–771.
23. Silva, R. C.; Gomez, A. M.; Diaz, S. F.; Lopez, F. T.; Elias, A. L.; Lopez, N. P.; Muramatsu, H.; Hayashi, T.; Fujisawa, K.; Kim, Y. A.; Endo, M.; Terrones, M. Formation of Nitrogen-Doped Graphene Nanoribbons *via* Chemical Unzipping. *ACS Nano* **2013**, *7*, 2192–2204.
24. Yang, W.; Liu, X.; Yue, X.; Jia, J.; Guo, S. Bamboo-Like Carbon Nanotube/Fe_3C Nanoparticle Hybrids and Their Highly Efficient Catalysis for Oxygen Reduction. *J. Am. Chem. Soc.* **2015**, *137*, 1436–1439.
25. Liu, M.; Song, Y.; He, S.; Tjiu, W.; Pan, J.; Xia, Y. Y.; Liu, T. Nitrogen-Doped Graphene Nanoribbons as Efficient Metal-Free Electrocatalysts for Oxygen Reduction. *ACS Appl. Mater. Interfaces* **2014**, *6*, 4214–4222.
26. Zheng, Y.; Jiao, Y.; Li, L. H.; Xing, T.; Chen, Y.; Jaroniec, M.; Qiao, S. Z. Toward Design of Synergistically Active Carbon-Based Catalysts for Electrocatalytic Hydrogen Evolution. *ACS Nano* **2014**, *8*, 5290–5296.
27. Xing, T.; Zheng, Y.; Li, L. H.; Cowie, B. C. C.; Gunzelmann, D.; Qiao, S. Z.; Huang, S.; Chen, Y. Observation of Active Sites for Oxygen Reduction Reaction on Nitrogen-Doped Multilayer Graphene. *ACS Nano* **2014**, *8*, 6856–6862.
28. Dommele, S. V.; Jong, K. P.; Bitter, J. H. Nitrogen-Containing Carbon Nanotubes as Solid Base Catalysts. *Chem. Commun.* **2006**, 4859–4861.
29. Wang, X.; Li, X.; Zhang, L.; Yoon, Y.; Weber, P. K.; Wang, H.; Guo, J.; Dai, H. N-Doping of Graphene through Electrothermal Reactions with Ammonia. *Science* **2009**, *324*, 768–771.
30. Medina, J. O.; Garcia, M. L.; Jia, X.; Gordillo, R. M.; Flores, M. A.; Swanson, D.; Elias, A. L.; Gutierrez, H. R.; Espino, E. G.; Meunier, V.; et al. Nitrogen-Doped Graphitic Nanoribbons: Synthesis, Characterization, and Transport. *Adv. Funct. Mater.* **2013**, *23*, 3755–3762.
31. Wei, J.; Lv, R.; Guo, N.; Wang, H.; Bai, X.; Mathkar, A.; Kang, F.; Zhu, H.; Wang, K.; Wu, D.; Vajtai, R.; Ajayan, P. M. Preparation of Highly Oxidized Nitrogen-Doped Carbon Nanotubes. *Nanotechnology* **2012**, *23*, 155601.
32. Gomez, A. M.; Diaz, S. M. V.; Gonzalez, V. J.; Lopez, F. T.; Silva, R. C.; Fujisawa, K.; Muramatsu, H.; Hayashi, T.; Mi, X.; Shi, Y.; et al. Clean Nanotube Unzipping by Abrupt Thermal Expansion of Molecular Nitrogen: Graphene Nanoribbons with Atomically Smooth Edges. *ACS Nano* **2012**, *6*, 2261–2272.
33. Zehtab Yazdi, A.; Chizari, K.; Sundararaj, U. Chemical Unzipping Process of Nitrogen-Doped Carbon Nanotubes. *29th International Conference of the Polymer Processing Society (PPS)* **2013**, Nuremberg, Germany, July 16–19.
34. Terrones, M.; Benito, A. M.; Manteca-Diego, C.; Hsu, W. K.; Osman, O. I.; Hare, J. P.; Reid, D. G.; Terrones, H.; Cheetham, A. K.; Prassides, K.; et al. Pyrolytically Grown BxCyNz Nanomaterials: Nanofibres and Nanotubes. *Chem. Phys. Lett.* **1996**, *257*, 576–582.
35. Dommele, S.; Romero-Izquirdo, A.; Brydson, R.; Jong, K. P.; Bitter, J. H. Tuning Nitrogen Functionalities in Catalytically Grown Nitrogen-Containing Carbon Nanotubes. *Carbon* **2008**, *46*, 138–148.
36. Rangel, N. L.; Sotelo, J. C.; Seminario, J. M. Mechanism of Carbon Nanotubes Unzipping into Graphene Nanoribbons. *J. Chem. Phys.* **2009**, *131*, 031105-1–031105-4.
37. Santos, R. P. B.; Perim, E.; Autreto, P. A. S.; Brunetto, G.; Galvao, D. S. On the Unzipping of Multiwalled Carbon Nanotubes. *Nanotechnology* **2012**, *23*, 465702.
38. Luque, G. L.; Rojas, M. I.; Leiva, E. P. M. Curvature Effect in the Longitudinal Unzipping Carbon Nanotubes: A DFT Study. *J. Solid State Electrochem.* **2013**, *17*, 1189–1200.

39. Xu, Z.; Bai, X.; Wang, Z. L.; Wang, E. Multiwall Carbon Nanotubes Made of Monochirality Graphite Shells. *J. Am. Chem. Soc.* **2006**, *128*, 1052–1053.
40. Dimiev, A. M.; Tour, J. M. Mechanism of Graphene Oxide Formation. *ACS Nano* **2014**, *8*, 3060–3068.
41. Stankovich, S.; Dikin, D. A.; Piner, R. D.; Kohlhaas, K. A.; Kleinhammes, A.; Jia, Y.; Wu, Y.; Nguyen, S. T.; Ruoff, R. S. Synthesis of Graphene-Based Nanosheets *via* Chemical Reduction of Exfoliated Graphite Oxide. *Carbon* **2007**, *45*, 1558–1565.
42. Dreyer, D. R.; Park, S.; Bielawski, C. W.; Ruoff, R. S. The Chemistry of Graphene Oxide. *Chem. Soc. Rev.* **2010**, *39*, 228–240.
43. Pei, S.; Cheng, H. M. The Reduction of Graphene Oxide. *Carbon* **2012**, *50*, 3210–3228.
44. Gao, X.; Jang, J.; Nagase, S. Hydrazine and Thermal Reduction of Graphene Oxide: Reaction Mechanisms, Product Structures, and Reaction Design. *J. Phys. Chem. C* **2010**, *114*, 832–842.
45. Liu, J.; Webster, S.; Carroll, D. L. Temperature and Flow Rate of NH_3 Effects on Nitrogen Content and Doping Environments of Carbon Nanotubes Grown by Injection CVD Method. *J. Phys. Chem. B* **2005**, *109*, 15769–15774.
46. Childres, I.; Jauregui, L. A.; Park, W.; Cao, H.; Chen, Y. P. Raman Spectroscopy of Graphene and Related Materials. In *New Developments in Photon and Materials Research*; Jang, J. I., Ed.; Nova Science Publishers: Hauppauge NY, 2013.
47. Sharifi, T.; Nitze, F.; Barzegar, H. R.; Tai, C. W.; Mazurkiewicz, M.; Malolepszy, A.; Stobinski, L.; Wagberg, T. Nitrogen Doped Multi Walled Carbon Nanotubes Produced by CVD-Correlating XPS and Raman Spectroscopy for the Study of Nitrogen Inclusion. *Carbon* **2012**, *50*, 3535–3541.
48. Bulusheva, L. G.; Okotrub, A. V.; Kinloch, I. A.; Asanov, I. P.; Kurenya, A. G.; Kudashov, A. G.; Chen, X.; Song, H. Effect of Nitrogen Doping on Raman Spectra of Multi-Walled Carbon Nanotubes. *Phys. Status Solidi B* **2008**, *245*, 1971–1974.
49. Zehtab Yazdi, A.; Fei, H.; Wang, G.; Tour, J. M.; Sundararaj, U. Boron/Nitrogen Codoped Helically Unzipped Multiwalled Carbon Nanotubes as Efficient Electrocatalyst for Oxygen Reduction. *ACS Appl. Mater. Interfaces* **2015**, *7*, 7786–7794.